Combining displacement, strain, temperature and heat source fields to investigate the thermomechanical response of an elastomeric specimen subjected to large deformations

Evelyne Toussaint, Xavier Balandraud, Jean-Benoît Le Cam, Michel Grediac

Combining displacement, strain, temperature and heat source fields to investigate the thermomechanical response of an elastomeric specimen subjected to large deformations

Evelyne Toussaint [a,c,*], Xavier Balandraud [b,c], Jean-Benoît Le Cam [d], Michel Grédiac [a,c]

[a] *Clermont Université, Université Blaise Pascal, Institut Pascal, BP 10448, 63000 Clermont-Ferrand, France*
[b] *Clermont Université, Institut Français de Mécanique Avancée, Institut Pascal, BP 10448, 63000 Clermont-Ferrand, France*
[c] *CNRS, UMR 6602, Institut Pascal, 63171 AUBIERE, France*
[d] *Université de Rennes 1, L.A.R.M.A.U.R – CNRS 6274, Campus de Beaulieu, Bât. 10B, 35042 RENNES Cedex, France*

Combining thermal and kinematic full-field measurements at the same time is gaining widespread acceptance in the community involved in the thermomechanical character-ization of materials. However, obtaining such attractive information in the case of elastomers for which large deformations occur raises specific experimental issues which are addressed in this paper. The problem arises in mapping both the thermal and the kine-matic quantities in the same reference coordinate system in order to write properly the heat diffusion equation. This equation provides heat sources which constitute a relevant quantity in the framework of thermomechanics. The procedure is presented and the underlying practical difficulties are detailed. It is then applied in the case of a specific test performed on a so-called three-branch specimen. Finally, the obtained strain and heat source distributions are briefly discussed.

1. Introduction

Full-field measurement techniques have recently spread in the experimental mechanics community. Some of these techniques enable their users to measure displacement and strain fields that occur in specimens subjected to a given test. Concerning elastomers, digital image correlation is probably the most suitable technique thanks to its ability to track points of the surface of specimens undergoing large deformations [1–3]. Another technique, termed infrared thermography, provides another field: the temperature variation field measured at the surface of specimens subjected to mechanical loads. These temperature variations can be due to various phenomena, including thermo-mechanical couplings. Temperature variations provide interesting information, but heat sources are an even more relevant quantity. Indeed, the temperature field is influenced by conduction as well as heat exchange with ambient air and grips. In practice, heat sources are deduced from the temperature variation fields using a numerical strategy based on a heat equation.

Both types of technique are generally used alone but there is an increasing interest in combining them. The main reason for this is the fact that strain and temperature or heat sources are often coupled and involved in advanced constitutive equations describing the thermo-mechanical response of materials, (see for instance [4] for elastomers). However, to the best of our knowledge only problems dealing with small strain amplitudes have been generally presented in the literature (see [5–8] for instance). Calculating heat sources in large deformations has been addressed in [9] but in that study only one IR camera was employed and a limited number of reflective points were tracked in infrared images during the test.

* Corresponding author. Clermont Université, Université Blaise Pascal, Institut Pascal, BP 10448, 63000 Clermont-Ferrand, France. Tel.: +33 473 288 073; fax: +33 473 288 027.
E-mail address: Toussaint@univ-bpclermont.fr (E. Toussaint).

The aim of the present paper is mainly to tackle specifically the issue of two types of measurements: displacement and temperature variations during the same test. The reason for this is that a certain number of problems arise in practice when both types of measurements are combined to obtain strain and heat sources maps in the same configuration. They arise in light of the fact that large deformations occur, that each type of camera features a sensor with a different size, that physical points of the specimen surface move during a test whereas the grid of measured points does not, that two configurations are involved (the reference and the current ones), and that numerical differentiation is needed to deduce strain and heat sources from the measurements.

The methodology is first presented in detail. It is then used to construct and to analyse the displacement, strain, temperature variation and heat source fields that take place in a three-branch specimen of complex shape subjected to a test presented recently in [10] for purposes of identification of constitutive parameters by processing heterogeneous strain fields.

2. Methodology

2.1. Calculation of heat sources

The aim of this section is to recall how to calculate heat sources in the Lagrangian configuration. Indeed, calculating the same quantity in the Eulerian configuration is really an issue because it requires more numerical calculations for the temporal differentiation of the temperature variation field, for the conduction term and for the description of the temperature field in the reference configuration in any deformed state considered, i.e. in any thermal image. In the following, the Lagrangian heat sources are calculated at any point of the specimen surface. For this purpose, the3D formulation of the heat diffusion is simplified using some assumptions that are briefly outlined here. The reader can refer to [3,11] for further information.

Considering the first and second principles of thermodynamics and assuming that Fourier's law is used to model heat conduction, the tridimensional heat diffusion equation can be written as follows:

$$\rho C_E \dot{T} - div(Kgrad\ T) - r = s \tag{1}$$

where ρ is the density, C_E is the specific heat at constant E, which is a measure of the deformation. ρ and C_E are assumed to by constant during deformation. K is the thermal conductivity tensor measured in the undeformed state, and r is the Lagrangian external heat source. The right-hand side s of Eq. (1) represents the heat sources produced by the material itself. It is composed of two terms that differ in nature:

- the thermomechanical couplings – For elastomeric materials, the heat sources due to thermomechanical couplings can be split into two terms: the effect of thermoelastic couplings [12] and the effect of microstructure changes such as crystallization (if any);
- the intrinsic dissipation, also termed mechanical dissipation (to be distinguished from the thermal dissipation in the Clausius-Duhem inequality) – This is due to mechanical irreversibilities such as viscosity or fatigue damage for instance.

Assuming that heat conduction can be considered as isotropic, Eq. (1) can be rewritten as follows:

$$\rho C_E \dot{T} - k\Delta T - r = s \tag{2}$$

where Δ is the Laplacian operator and k the conductivity coefficient which replaces the thermal conductivity tensor K in the case of isotropy. Assuming that the specimen is flat, integrating the heat diffusion Eq. (2) over the specimen thickness and using the temperature variation leads to the following bidimensional formulation of the heat diffusion equation [13]:

$$\rho C_E \left(\dot{\theta} + \frac{\theta}{\tau} \right) - k\Delta_{2D}\theta = s \tag{3}$$

where Δ_{2D} is the two-dimensional Laplacian operator. τ is a time constant which characterizes the heat exchanges by convection with ambient air in the direction perpendicular to the specimen plane. Assuming that the exchanges by convection are simply proportional to the temperature variation θ, this quantity is defined by:

$$\tau = \frac{e\rho C_E}{2h} \tag{4}$$

where e is the specimen thickness, h is the convection coefficient. As a first approximation, τ is considered here as a constant. Its value can be estimated from simple tests of natural return to room temperature. In the present study, it value is equal to 30 s. It must be noted that the heat sources classically expressed in $W \cdot m^{-3}$ can also be expressed in $^{\circ}C \cdot s^{-1}$ by dividing the heat sources by ρ C_E. This last unit is often considered to be more suitable for interpreting the heat source. Thus, Eq. (3) becomes:

$$\frac{d\theta}{dt} + \frac{\theta}{\tau} - D\Delta_{2D}\theta = \frac{s}{\rho C_E} \tag{5}$$

where D is the thermal diffusivity which is equal to $k/\rho C_E$. For elastomers, the order of magnitude of D is very low. As a consequence for a short duration test, the conduction term is negligible in Eq. (5). Hence, the simplified heat equation diffusion used in the present study writes as follows:

$$\frac{d\theta}{dt} + \frac{\theta}{\tau} = \frac{s}{\rho C_E} \tag{6}$$

A motion compensation technique is required to calculate heat sources from Eq. (6). This compensation allows us to associate a displacement and a temperature at any point of the surface of a specimen in the reference configuration, chosen here to be the undeformed state. This motion compensation technique is presented in Section 2.2 and is used for determining the temperature field variations θ.

2.2. Motion compensation technique

The objective here is to explain in detail how thermal maps that are measured in the deformed configuration are mapped in the reference configuration.

- Step 1: the starting point is the fact that two back-to-back cameras are employed. Assuming digital image correlation is used to measure the displacement/strain fields, the CCD camera captures the grey level distribution on one of the two faces of the specimen. Processing the image of the grey level distribution on the deformed and reference surfaces enables one to deduce the displacement field. This displacement is generally known at the centre of each element of a regular mesh, each element being the so-called zone of interest (ZOI) over which correlation between the current and the reference image is calculated. The size of each ZOI is a few pixels, so the displacement field is not determined at any pixel of the sensor of the camera, but at a much lower number of points which is equal to the number of ZOIs. With most digital image correlation (DIC) software, this displacement field can be represented either in the current or in the reference configuration.

The second camera is an infrared camera which captures the temperature variation distribution on the opposite face. These data are, therefore, known for the current configuration. The sensors of these cameras do not capture exactly the same scene, so the first step is to know exactly the correspondence between the two zones. The scenes must therefore be chosen in such a way that they share a common feature (for instance at least a particular point of the specimen edge), so it is then possible to localize one scene with respect to the other. Second, it is necessary to know the dimension of the pixels of each of the sensors. This calibration can easily be performed, for instance by dividing the actual initial width of the specimen (assuming the whole width is seen by both cameras) by the number of pixels of each of the sensors;

- Step 2: each displacement scene being now localized with respect to the corresponding thermal one, the second step is to consider the displacement field, which is known over a certain grid. The pitch of this grid is the size of the ZOI, which is often equal to several pixels of the CCD camera. This grid can either be known in the reference or the deformed coordinate system but it is generally different to that of the infrared camera. In practice, since DIC is performed on ZOIs the dimensions of which are greater that the pixel of the infrared camera, the next step is to interpolate the displacement field in such a way that this quantity becomes known over the same grid as that of the infrared camera. This is performed on the displacement field known on the current coordinate system. In practice, using Matlab [14] in this study, this can be simply done by using, for instance, the *griddata* function. Fig. 1a and b represent a typical example of a portion of the displacement field plotted on the deformed grid given by the DIC system, and Fig. 1c and d the same field mapped on the thermal grid. The deformed grid given by the DIC system is also interpolated on the thermal grid. Finally, the undeformed grid mapped on the thermal grid is obtained by subtracting the displacement field interpolated on the thermal grid from that interpolated on the deformed thermal grid.
- Step 3: the last step is to plot the temperature field in the reference coordinate system, since at this stage both the current and the initial temperatures are known in the current coordinate system. The reason for this is that the infrared camera sensor remains fixed, whereas the physical points of the front face where the temperature measurement is performed move during the test. Since both the temperature and the displacement fields are known exactly on the same grid thanks to the preceding

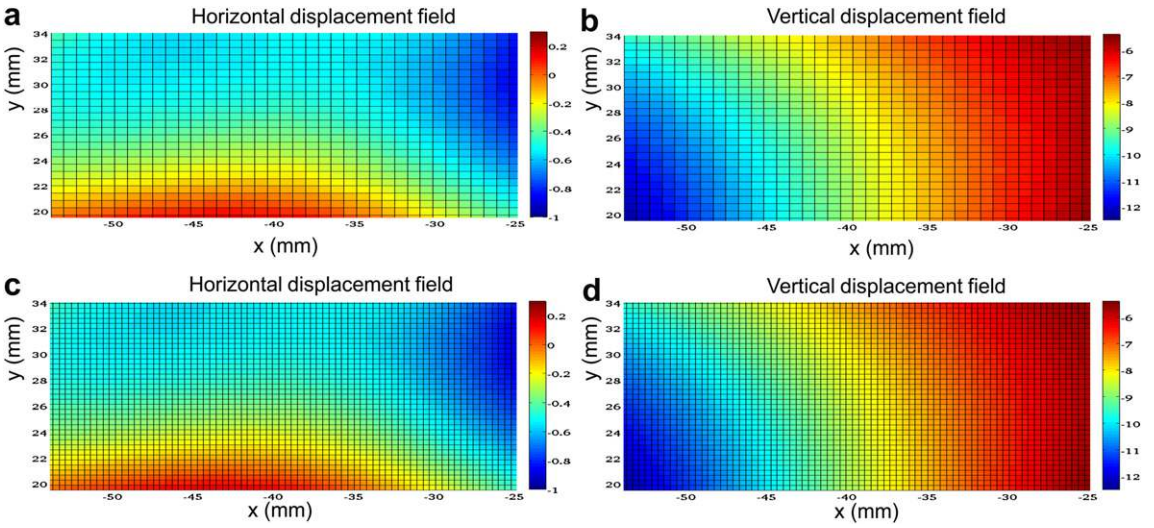

Fig. 1. Example of a displacement field: a) and b) obtained with displacement grid, c) and d) interpolated on the thermal grid.

step, this new map is obtained by combining both fields. Fig. 2a presents an example of a portion of the temperature field in the deformed configuration. This temperature field is then mapped in the reference coordinate system (Fig. 2b). It is worth noting here that the initial shape of this zone is a rectangle since this information is known over the sensor grid of the infrared camera, but it is not a regular grid anymore after application of this procedure. It is, therefore, necessary to interpolate again this result in such a way that it becomes known over the same regular grid as that of the displacement field, as illustrated in Fig. 2c. It can be seen that the interpolation causes a slight smoothing of the temperature field. The dotted line in Fig. 2c corresponds to the border of the zone presented in Fig. 2b to show that. The temperature fields in the adjacent zones must be known to reconstruct the temperature field in a regular rectangle.

- Step 4: the same procedure as above is applied to the reference temperature field. The temperature field variations θ is, therefore, known in the undeformed configuration by simply subtracting both the current and the initial temperature fields. This is possible since both are now known over the same grid.

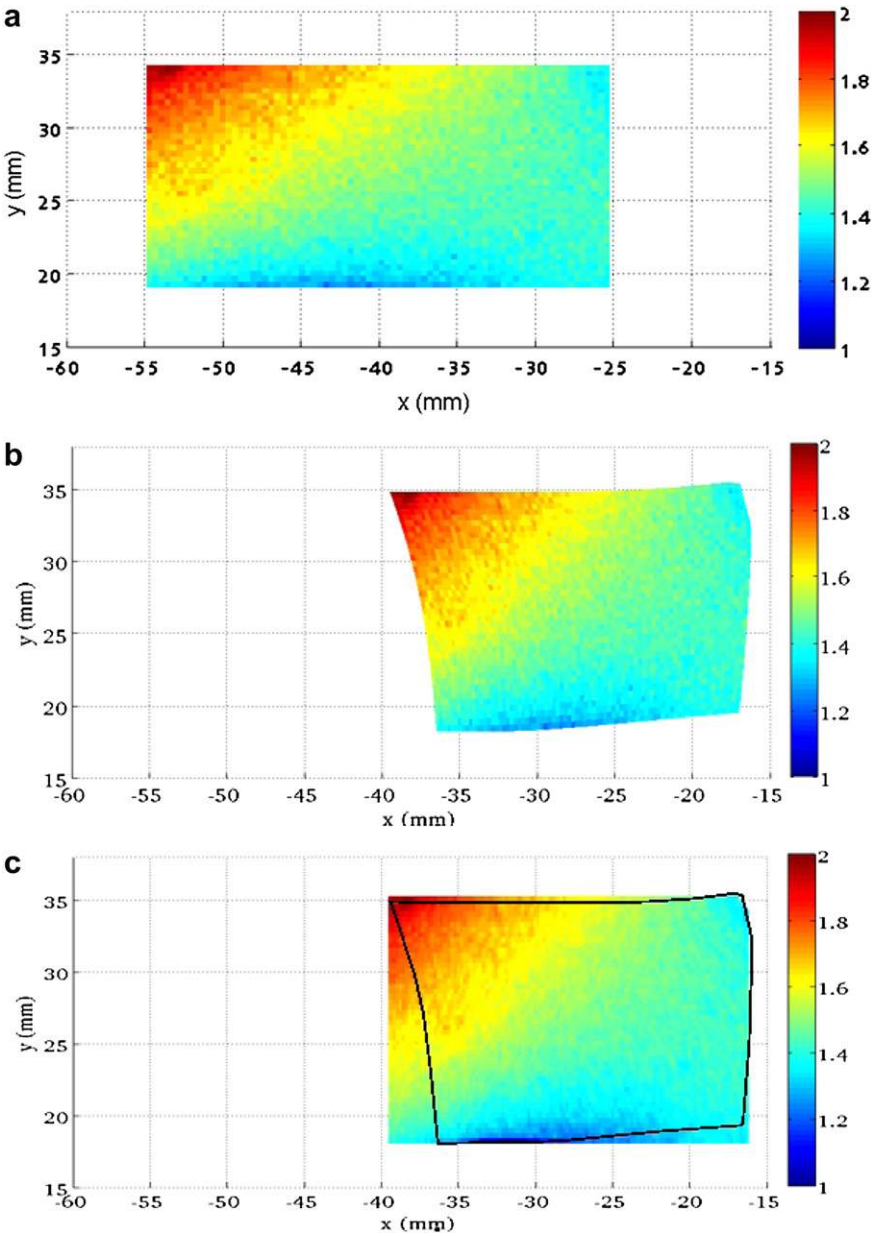

Fig. 2. Example of temperature field in: a) deformed configuration, b) undeformed configuration and c) undeformed configuration interpolated on a regular grid.

3. Application to the three-branch test

The objective now is to illustrate the procedure described above to construct the strain, displacement, temperature variation and heat source fields in the same configuration. These fields, which are rather complex, are then discussed.

3.1. Material and experimental setup

The material considered here is a carbon black filled natural rubber (CB-NR). The three-branch specimen was initially developed in a previous work to induce tensile, compression and equibiaxial tension [10]. The corresponding experimental setup is shown in Fig. 3. One can distinguish two back-to-back cameras: a CCD camera and an IR camera. The geometry of the specimen is presented in Fig. 4. In practice, branches 1 and 2 (see Fig. 4) of the specimen were fastened to the grips of a conventional testing machine, whereas branch 3 (see Fig. 4) was fastened in a specific grip aligned in the horizontal direction. The specimen geometry was 2 mm thick, 52 mm long, and the branches were 20 mm in width. This geometry corresponds to the undeformed state of the specimen, which is considered as the reference configuration in the present study. It is also depicted in Fig. 5a, which corresponds to the undeformed specimen. Branch 1 being clamped, the loading was applied by prescribing a displacement along the vertical axis defined by branches 2 and 3.

3.2. Loading conditions

The test was carried out with a 'MTS 858 Elastomer Test System' testing machine (see Fig. 3). Its loading capacity is $\pm$ 15 kN and that of the load cell $\pm$ 1 kN. A test device suitable for the testing machine was designed in order to apply such biaxial loadings, i.e. to generate equibiaxial tension and pure shear at the specimen centre, [10]. The loading was applied in two steps (see Fig. 5):

- the first step of the test consisted of applying a 12 mm – displacement along the y-direction and a 30 mm – displacement along the x-direction. During this step, images were stored with a CCD camera in order to calculate displacement fields. Then, a 5 min pause enabled us to ensure that the specimen returned to thermal equilibrium before starting the next step. The configuration obtained at the end of the first step is referred to as the intermediate configuration in the following (see Fig. 5b);
- the second step consisted of applying a 47 mm – displacement along the y-direction. The displacement rate was equal to 15.7 mm/s. This rate is significant to guarantee sufficiently high temperature variations on the surface of the specimen. Both the displacement and the thermal measurements were performed simultaneously on two opposite sides of the specimen during this step. At the end of the test, the corresponding global stretch ratios were 1.85 and 2.13 along the x and y-directions, respectively. The third configuration, which corresponds to the current geometry at any time during step 2, is called the current configuration. This configuration is illustrated by the schematic view in Fig. 5c in a particular case: the end of step 2.

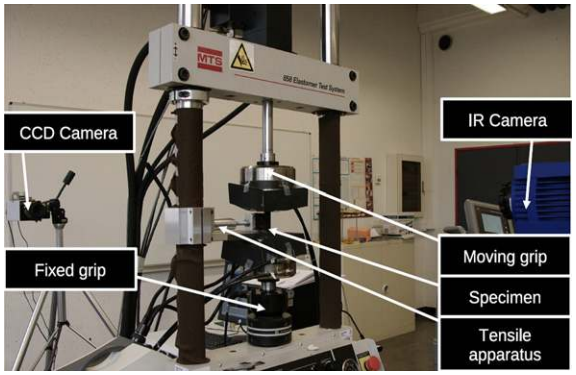

Fig. 3. Experimental set-up.

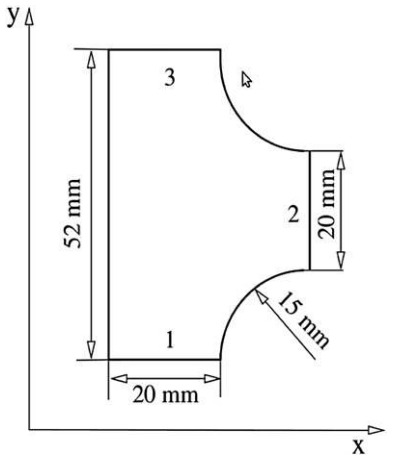

Fig. 4. Specimen geometry.

3.3. Measuring of the displacement fields

The images captured by the CCD camera were stored using a cooled 12-bit dynamic Sensicam camera. The images correspond to various stretch ratio levels. The CCD sensor of the camera features $1376 \times 1040 \approx 1.4\ 10^6$ connected pixels. The surface of the specimen was illuminated by three flexible and movable light guides fed by a KL 2500 LCD cold light source which provided uniform lighting. The DIC technique was used to measure the displacement field on the specimen surface [15]. This method consists of matching, before and after displacement, the brindled pattern on a physical part of the observed surface of the specimen termed "Region Of Interest" (ROI). The SeptD software was used for this purpose [16]. DIC was carried out with a resolution of 0.03 pixel, corresponding to 2.9 μm, and a spatial resolution (defined as the smallest distance between two independent points) of 10 pixels, which corresponds here to 975 μm. A set of sub-images was

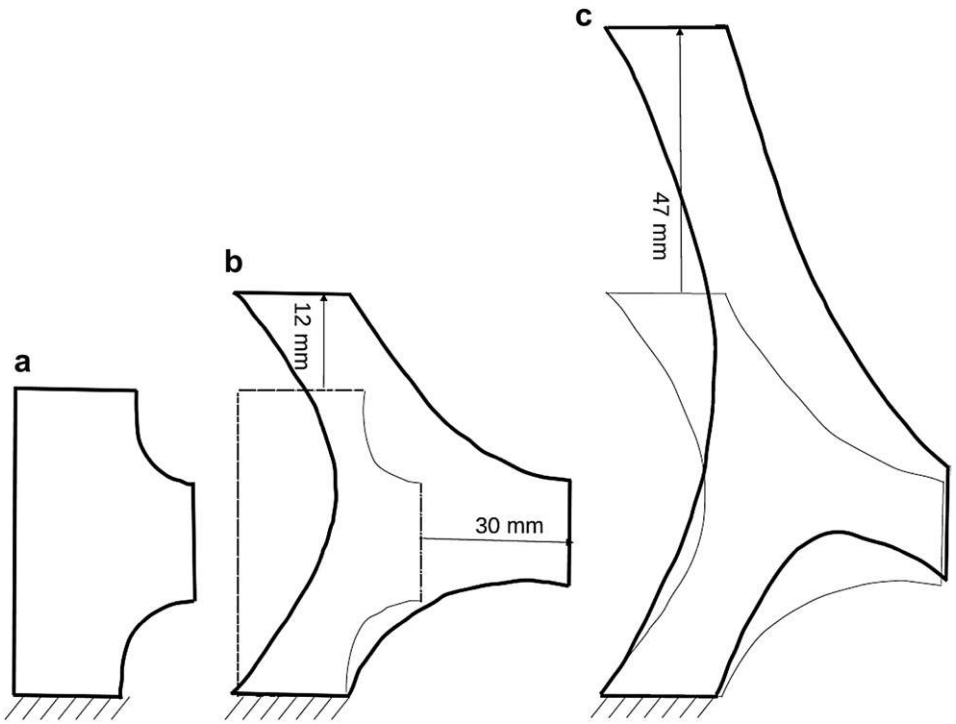

Fig. 5. Configurations: a) reference; b) intermediate; c) current (here at the end of step 2).

considered to determine the displacement field of a given image with respect to a reference image. This set is referred to as the 'Zone of Interest' (ZOI). A correlation function was used to calculate the displacement of the centre of a given ZOI between two images captured at different loading steps. White paint was sprayed on the specimen surface before testing to improve the contrast of the images.

3.4. Measurement of thermal fields

Temperature measurements were carried out with a Cedip Jade III-MWIR infrared (IR) camera which features a local plane array of 320 $\times$ 240 pixels and detectors with a wavelength range of 3.5–5 μm. The integration time was 1500 μs and the acquisition frequency was set to 150 Hz.

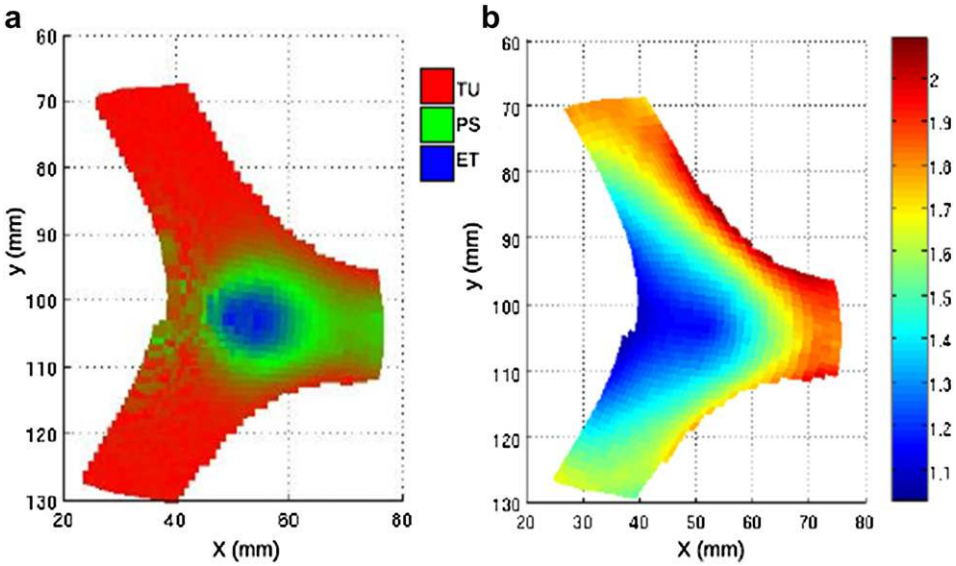

Fig. 6. Heterogeneity of the test at the end of step 1 in intermediate configuration: a) loading cases, b) maximum stretch ratio λ_{max} in the gauge section.

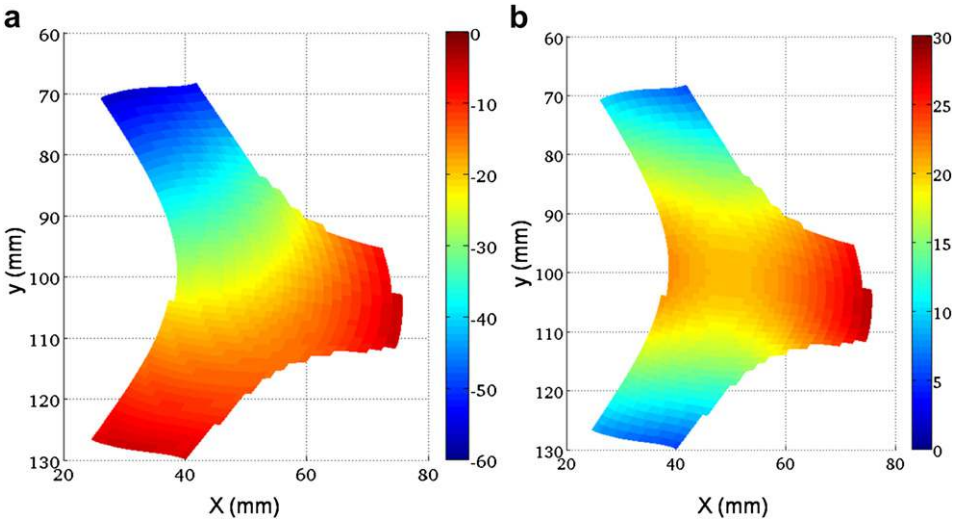

Fig. 7. Displacement fields at the end of the second step in intermediate configuration: a) horizontal displacement, b) vertical displacement.

The noise equivalent temperature difference (NETD) of the measurement, in other words the thermal resolution, is equal to about 20 mK for the temperatures observed in the present study, which range between 5 and 40 °C. In order to ensure that the internal temperature of the camera was optimal for performing the measurements, it was set up and switched on four hours before the experiment. The spatial resolution in temperature was equal to 380 μm. This value is equal to the pixel size projected on the specimen.

The initial temperature field was measured at the end of the first step (intermediate configuration). It was nearly homogeneous and equal to the ambient temperature. The small differences with the ambient temperature are due to the fact that the moving grip was warmer than the fixed vertical and horizontal ones. This initial temperature field was used to obtain the temperature variation maps during the second step, as explained below.

3.5. Heterogeneity of the test

The heterogeneity of the test at the end of the first step can be observed in Fig. 6, which shows the loading conditions as functions of the (X, Y) coordinates defined in the intermediate configuration obtained at the end of the first step. In Fig. 6a, the Equibiaxial Tensile (ET), Pure Shear (PS) and Uniaxial Tensile (UT) loading conditions correspond to the blue, green and red colours, respectively. For the sake of simplicity, intermediate states of stress are defined by a colour which is a weighted average of two colours, namely, blue and green for the loading conditions between ET and PS, green and red for the loading conditions between PS and UT. For such a test, the central zone of the specimen is mainly subjected to ET loading conditions and the zones corresponding to the three branches are mainly subjected to UT loading conditions. The PS zone is located within a ring-shaped zone located between the ET and UT zones. Some additional information on the heterogeneity induced by the test can be provided by the distribution of the maximum stretch ratio λ_{max}. Fig. 6b shows the distribution of this quantity. The lowest and highest values of λ_{max} are equal to 1.07 and 2.09, respectively. It is observed that the lowest values of λ_{max} are located in the ET zone, whereas the highest values are located in the UT zone, near to the boundary of the specimen located between branches 2 and 3.

3.6. Displacement field measured by DIC

Typical horizontal and vertical displacement fields obtained at the end of the second step have been plotted in the intermediate configuration. They are shown in Fig. 7a and b, respectively. As explained in Section 2.2, the

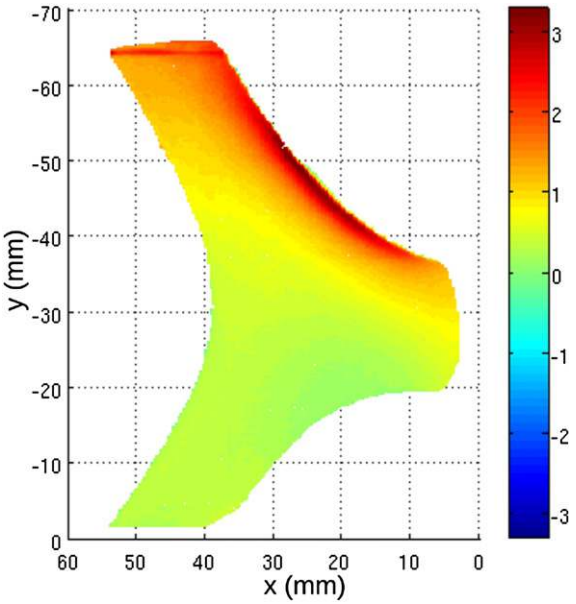

Fig. 8. Temperature variation field θ at the end of step 2 in °C. The field is plotted in the intermediate configuration for comparison purpose with the maps presented in other figures.

displacement fields that occur during the test are needed to establish the correspondence between the location of the material points of the specimen at any stage of the loading (current configuration) and at the end of step 1 (intermediate configuration). It is then possible to correctly analyse and process the temperature maps at different loading amplitudes in the intermediate configuration. Using the current motion compensation technique, one can analyse temperature variation field θ and the corresponding heat sources.

3.7. Analysis of temperature variation fields

Fig. 8 shows the temperature variation field θ at the end of the loading procedure, i.e. at the end of the second step. The lowest temperature variations are observed in branch 1. The highest values are observed in branch 2, especially at the right-hand side boundary. The temperature variation reaches more than 3 °C. It can be noted that this zone of high temperature variations is mainly obtained in the UTzone (see Fig. 6a).

The temperature variations in the specimen are the consequence of the heat sources produced by the material due to stretch. Steps 1 and 2 of the present test induce large deformations of rubber. As the filled natural rubber considered here is crystallizable, the heat source produced by the material during step 2 is due to thermoelastic couplings and, possibly, to stress-induced crystallization, which is an exothermic phenomenon.

For the material considered here and for a uniaxial tensile test (UT), the crystallization starts at $\lambda_{max} = 1.64$ [17,18]. It can be noted that this value is greater in some zones under UT loading, for example in branch 3 of the specimen (see Fig. 6). Consequently, the increase in temperature is due to the effects of both the thermoelastic couplings and the stress-induced crystallization. The results are now analysed in terms of heat sources.

3.8. Analysis of heat sources

Fig. 9 presents the heat source maps at four times regularly distributed along step 2: at 0, 1, 2 and 3 s. The maps show the progressive increase of the heat sources vs. time, especially in zone A of the specimen (see Fig. 9d). Values of heat source in branch 1 slightly increase vs. time, even if it is not distinguishable with the colour scale in

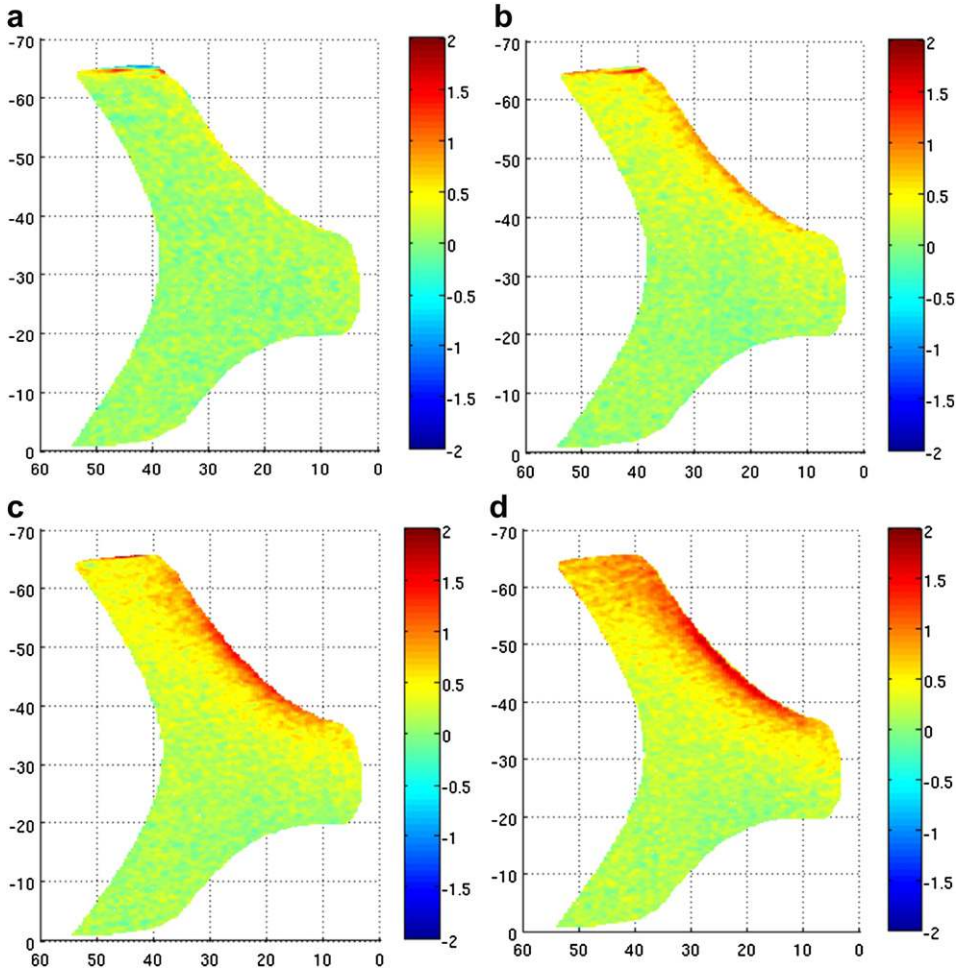

Fig. 9. Evolution of heat sources (in $°C \cdot s^{-1}$) during step 2. All fields are plotted in the intermediate configuration for comparison purpose with the maps presented in other figures. a) at t = 0 s, b) at t = 1 s, c) at t = 2 s, d) at t = 3 s.

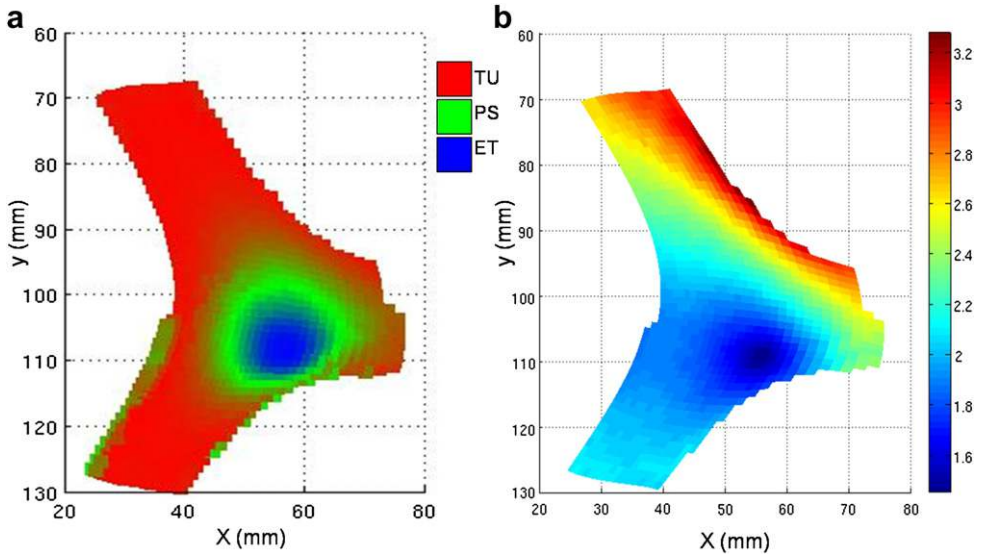

Fig. 10. Heterogeneity of the test at the end of step 2 in intermediate configuration: a) loading conditions, b) maximum stretch ratio λ_{max} in the gauge section.

Fig. 9. However, the trend was checked. It is interesting to compare the fields of heat sources (Fig. 9d), the loading conditions (Fig. 10a) and the maximum stretch ratios (Fig. 10b) at the end of step 2, especially in zone A. The heat sources appearing in red in Fig. 9d correspond to UT loading (Fig. 10a) and to the maximum stretch ratios (Fig. 10b). This zone can be distinguished from others by its heat production. Indeed, as it has already been observed in the previous section, this result is probably due to the effects of thermoelastic couplings and to those of crystallization which occur at the same time. It can be noted that no large increases of heat sources were detected in PS and ET zones for the achieved stretch ratios levels. Finally, some comments related to the zones subjected to ET, PS, intermediate states and UT in branch 1 are made. Few heat sources are significantly visible in these zones. The present test enables us to say that the maximum stretch ratios locally reached (see Fig. 10b) in these zones are too low to produce an amount of latent heat detectable with the technique used.

4. Conclusions

Measuring simultaneously the displacement, strain, temperature variation and heat source fields on the surface of elastomeric specimens subjected to mechanical test provides very interesting information on their complex thermo-mechanical responses. However, obtaining these quantities raises specific practical problems that are addressed in this paper. It is shown that it is possible to map all these quantities in a given configuration, the reference configuration, by using specific and suitable interpolations. The procedure was then used to calculate these fields in a three-branch specimen which sustains a complex state of stress. Further work will deal with the simultaneous use of these fields to identify the whole set of parameters governing advanced models describing the thermo-mechanical of elastomers, in the same spirit of inverse methods based on strain or displacement fields only (see [10] for instance).

Acknowledgements

The authors would like to thank Dr. Manuel Buisson for his collaboration and fruitful discussions.

References

[1] M.-C. Lafarie-Frenot, F. Lagattu, J. Brillaud, High strain gradient measurements by using digital image correlation technique, Materials Characterization 53 (2004) 17–28.
[2] D. Favier, L. Orgéas, P. Vacher, L. Meunier, G. Chagnon, Mechanical experimental characterization and numerical modelling of an unfilled silicone rubber, Polymer Testing 27 (2008) 765–777.
[3] Le Cam J.-B. A review of the challenges and limitations of full-field measurements applied to large heterogeneous deformations of rubbers. Strain, Article first published online: 2 Mar 2012 http://dx.doi.org/10.1111/j.1475-1305.2011.00830.x.
[4] P. Chadwick, Thermo-mechanics of Rubberlike Materials, A276, PhilosophicalTransactions of the Royal Society, London, 1974, 371.
[5] A. Chrysochoos, B. Wattrisse, J.-M. Muracciole, Y. El Kaim, Fields of stored energy associated with localized necking of steel, Journal of Mechanics of Materials and Structures 4 (2009) 245–262.
[6] P. Schlosser. Influence des aspects mécaniques et thermiques sur les mécanismes de déformation des alliages NiTi. PhD thesis, Université Joseph Fourier, Grenoble, 2008.
[7] T. Sakagami, T. Nishimura, T. Yamaguchi, N. Kubo, Development of anew motion compensation technique in infrared stress measurement based on digital image correlation method, Transactions of the Japan Society of Mechanical Engineers (2006).
[8] K. Lavernhe-Taillard, A. Maynadier, M. Poncelet, S. Roux, One-shot measurement of thermal and kinematic fields: infrared image correlation (iric), Experimental Mechanics 52 (2012) 241–255.
[9] T. Pottier, M.P. Moutrille, J.-B. Le Cam, X. Balandraud, M. Grédiac, Study on the use of motion compensation techniques to determine heat sources. Application to large deformations on cracked rubber specimens, Experimental Mechanics 49 (2009) 561–574.
[10] T. Guélon, E. Toussaint, J.-B. Le Cam, N. Promma, M. Grédiac, A new characterization method for rubber, Polymer Testing 28 (2009) 715–723.
[11] A. Chrysochoos, V. Huon, F. Jourdan, J.-M. Muracciole, R. Peyroux, B. Wattrisse, Use of full-field digital image correlation and infrared thermography measurements for the thermomechanical analysis of material behaviour, Strain 46 (2010) 117–130.

[12] G.A. Holzapfel, Nonlinear Solid Mechanics: A Continuum Approach for Engineering, John Wiley and Sons, 2000.
[13] A. Chrysochoos, H. Louche, An infrared image processing to analyse the calorific effects accompanying strain localisation, International Journal of Engineering Science 38 (2000) 1759–1788.
[14] Matlab: A Practical Introduction to Programming and Problem Solving, Butterworth-Heinemann Ltd, 2011.
[15] M.A. Sutton, W.J. Wolters, W.H. Peters, W.F. Ranson, S.R. Mc-Neil, Determination of displacements using an improved digital correlation method, Image and Vision Computating 1 (1983) 133–139.
[16] P. Vacher, S. Dumoulin, F. Morestin, S. Mguil-Touchal, Bidimensional strain measurement using digital images, in: Proceedings of the Institution of Mechanical Engineers. Part C: Journal of Mechanical Engineering Science (1999).
[17] J.-B. Le Cam, E. Toussaint, Volume variation in stretched natural rubber: competition between cavitation and stress-induced crystallization, Macromolecules 41 (20) (2008) 7579–7583.
[18] J.-B. Le Cam, E. Toussaint, Cyclic volume changes in rubber, Mechanics of Materials 41 (2009) 898–901.